JOURNAL OF MATERIALS SCIENCE 21 (1986) 4233–4244

Analysis of the solidified structure of rheocast and VADER processed nickel-base superalloy

D. APELIAN*, J.-J. A. CHENG‡
*Department of Materials Engineering and ‡Solidification Processing Laboratory, Drexel University, Philadelphia, Pennsylvania 19104, USA

Conventional "ingot" processing of highly alloyed compositions results in a cast product which suffers from extensive macrosegregation, hot tears, and heterogeneities. By controlling the solidification journey, one can produce a fine grained cast product. This is achieved by manipulating the melt in the mushy zone. Rheocasting and vacuum arc double electrode remelting (VADER) are two such technologies where the melt is processed in the mushy zone. IN–100, a nickel based superalloy, was rheocast as well as VADER processed. The resultant cast structures are analysed, compared and discussed both on micro- and macrostructural levels. The effect of the rheocast processing variables (stirring speed, time and temperature) on the cast microstructure are also discussed

1. Introduction

In the late 1960's gas turbine disc materials with increasing strength and operating temperature capabilities were introduced to meet high performance engine requirements, such as IN–100, MERL 76 and Rene 95 which are nickel-base alloys. Conventional "ingot" processing techniques such as vacuum arc remelting (VAR) of these highly alloyed compositions results in a cast product which suffers from massive segregation, heterogenities, coarse grains, hot tears, and, in brief, a product which cannot be further processed and worked. The challenge is then to produce a cast product which does not contain massive heterogenities and defects, and a cast product which can be further processed.

One alternative is to resort to powder metallurgy (P/M) processing which leads to homogeneous fine grained structures. Since each powder particle is a "microcasting", the extent of chemical segregation is restricted to the maximum powder particle size. These powders can be consolidated by a variety of techniques such as Gatorizing [1]; however, the processing and manufacturing operations are complex and expensive. In addition, high operating stress levels and long operating lives require a high level of material cleanliness to reduce inadvertent inclusions in the component [2]. Unfortunately, P/M processing includes many steps where the powders are "handled" and are thus prone to contamination.

Other alternative approaches include the production of fine-scale microstructures by processes such as vacuum arc double electrode remelting (VADER) and rheocasting (stircasting) where the solidification phenomenon is closely controlled. The VADER melting process, developed by Special Metals Corporation (New Hartford, New York), allows one to produce small, crack-free ignots with fine grain size and low levels of chemical segregation [3]. Similarly, ingots of fine equiaxed non-dendritic structure with reduced shrinkage and segregation can also be produced by the rheocasting process which was developed by Flemings *et al.* [4–6]. Structural characteristics inherent to both the VADER and rheocasting processes are recognized as factors which might improve the properties and performance of the turbine disc or permit the direct processing of ingots to shape components.

In this paper, we analyse, compare and discuss the solidification structures of rheocast, VADER processed and conventionally processed (non-stirred) IN–100 ingots. The analysis was carried out at both micro- and macrostructural levels.

2. Background

The simplest nickel-base superalloys contain chromium, aluminium, titanium, carbon, boron and zirconium, and the most complex alloys contain several of these additional elements: cobalt, molybdenum, tungsten, tantalum, iron, vanadium, niobium and hafnium [7]. The main phases present in the structure of these alloys are the alloy matrix γ, precipitated phase γ' and carbides. The γ' phase has an ordered fcc ($L1_2$ type) structure and precipitates coherently in the fcc γ matrix [8]. Various types of carbides may exist, and in addition other phases such as borides [8], tcp type phases [9] and grain boundary γ' [10] can also be present. The strength of these alloys is mainly influenced by solid solution hardening of the matrix γ, and by precipitation hardening due to γ' precipitates [11]. The two specific processes which are the subject of this study, VADER and rheocasting, are reviewed below.

2.1. Vacuum arc double electrode remelting (VADER)

The VADER process, patented by Special Metals Corporation [12] is a potential alternative to P/M processing; a schematic diagram of the process is shown in Fig. 1. In VADER, an arc is established between two consumable electrodes and the molten

0022–2461/86 $03.00 + .12

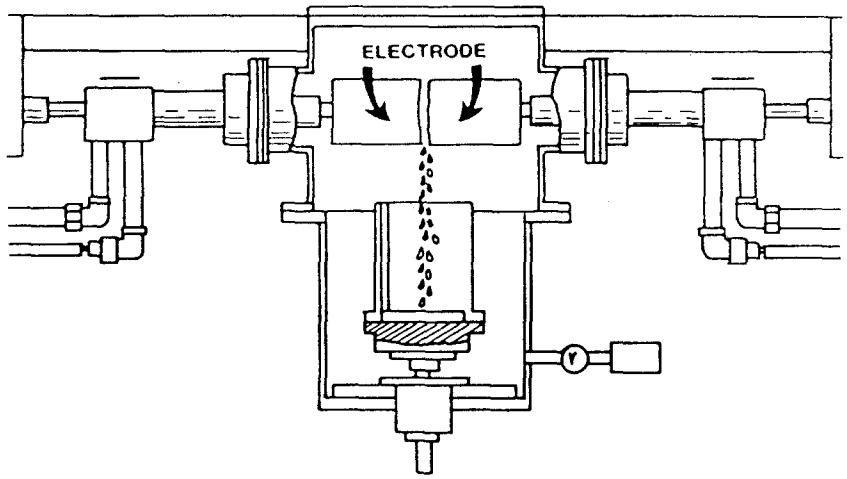

Figure 1 Schematic diagram of the VADER melting process.

metal is allowed to drip into a stationary, rotating or withdrawing mould located beneath the electrodes. The metal drips from faces of two electrodes and essentially these droplets are consolidated *in situ* in the mould. Droplet temperature measurements indicate that they are slightly below the liquidus temperature of the alloy, e.g. droplet temperature measurements on IN–718 alloy were found to be 11° C below the liquidus temperature as measured by differential thermal analysis (DTA) [13]. Accordingly, the metal droplets contain solid particles or nuclei as they fall into the mould and form a slurry puddle [11]. The formation of fine grained VADER castings are explained based on the idea of numerous nuclei being present in the semi-liquid mass at the onset of solidification and subsequent grain growth being interfered by precipitated phases. The VADER process has the following benefits compared to the conventional VIM–VAR processing route [3]: (i) uniform fine grain size (typically 100 μm), (ii) reduced macrosegregation, (iii) less prone to internal cracking, (iv) improved hot workability, (v) more energy efficient than VAR.

2.2. Rheocasting

Rheocasting was developed by Flemings *et al.* [14]. Rheocast slurries are thixotropic and show a hysteresis loop phenomenon similar to other well known thixotropic systems [15]. Briefly, in rheocasting the melt is cooled through the mushy zone, it is mechanically stirred and subsequently the melt (now a slurry) is held at a given temperature (corresponding to a certain fraction solid) while it is continuously sheared. Rheocast metal has been produced continuously at volume fractions solid ranging up to about 70% [14]. After shearing, the rheocast slurry may be cast into a receiving crucible such as through bottom pouring or it may be allowed to solidify in the crucible. The following alloys have been successfully rheocast: Al–base [16–18], Cu–base [19], Pb–Sn [20], Fe–base [21], Co–base [22] and Ni–base [23] alloys. The basic rheocasting concept has been extended to produce composite materials and wrought-slurry castings similar to squeeze casting. Processes derived from the rheocasting process are compocasting, thixocasting and thixoforging [14].

The conventional dendritic structure is altered by manipulating the processing conditions. There are several ways one can obtain a fine equiaxed grain structure. For example, Kattamis *et al.* [24] have shown that magnesium alloys, grain refined by zirconium catalysts, exhibit a spherical morphology where grains have a size equal to that of the dendrite arms. In rheocasting, on the other hand, the dendrite arms are fragmented and a cast structure having an equiaxed non-dendritic morphology is produced [15, 20].

Rheocast structures are affected by four independent variables: shear rate, cooling rate, stirring time and temperature (or volume fraction solid particles). The following observations were made on castings which were stirred in the mushy zone and subsequently water quenched [14, 16, 18, 25]:

1. The primary solid particle size decreases as the shear rate, cooling rate or stirring time increases. In addition, as the volume fraction solid increases, one observes larger primary solid particles.
2. Increasing shear rate, stirring time or volume fraction solid results in an increase in the sphericity of the primary solid particles.

Furthermore, rheocast structures offer the following advantages over conventional cast structures [13, 14]:

1. reduced shrinkage and potential of crack formation;
2. microporosity, if present, is uniformly distributed;
3. formation of a fine and non-dendritic grain structure;
4. reduced segregation.

Hypotheses such as dendrite arm remelting, mechanical fracture of dendrite arms and enhanced nucleation, have been reported as mechanisms giving rise to the rheocast structure. Unfortunately, none of these has been confirmed. Vogel *et al.* [26, 27], however, have proposed a model for the fragmentation of dendrites during stirring based on the formation of high-angle grain boundaries in dendrites following bending of the arms. Due to dendrite fragmentation, the effect of stirring would change the primary solid particle morphology from a pure dendritic to a spherical one. This model, known as the Vogel–Doherty–Cantor model, has been subsequently studied and confirmed by Lee [18]. Recently, Doherty *et al.* [25] reviewed the

TABLE I Composition of differently processed IN–100 alloys (wt %)

	As-received (VIM cast)	VADER cast	rheocast
Nickel	55.37	55.28	55.53
Cobalt	18.85	18.78	18.67
Chromium	12.08	12.38	11.99
Aluminium	4.98	4.90	4.95
Titanium	4.56	4.43	4.63
Molybdenum	2.99	3.17	3.01
Vanadium	0.78	0.65	0.79
Iron	0.13	0.12	0.14
Tantalum	0.10	0.10	0.10
Tungsten	0.10	0.10	0.10
Carbon	0.06	0.07	0.06
Silicon	0.05	0.05	0.05
Niobium	0.05	0.05	0.05
Zirconium	0.04	0.05	0.04
Boron	0.012	0.01	0.013
Manganese	0.01	0.01	0.01
Copper	0.01	0.01	0.01
Oxygen	0.006	0.001	0.005
Nitrogen	0.001	0.001	0.001

literature on the development of rheocast structure and have presented some new evidence in support of Vogel's model.

3. Experimental procedure

3.1. Materials

The nominal composition of the as-received IN–100 ingot which was subsequently rheocast is shown in Table I. The as-received ingots were VIM melted and cast at Cannon–Muskoegan Corporation (Muskoegan, Michigan, USA). The VADER ingot was processed at and purchased from Special Metals Corporation, New Hartford, New York. The composition of the VADER ingot is also given in Table I.

3.2. Solidification apparatus and processing

3.2.1. Rheocasting of IN–100 nickel base superalloy

A GCA vacuum hot-press furnace was modified to a high vacuum rheocasting furnace. A ferrofluidic vacuum rotary feed through seal was used which transmitted 100% positive rotation into the vacuum chamber by means of a solid through-shaft design and a ferrometric (magnetic) seal. A detailed schematic of the crucible assembly is shown in Fig. 2 where the various components are indicated. The crucible is held down by a stainless steel plate and is immobile while the paddle is rotated.

The charge was induction melted in a crucible. At the top position of the vacuum chamber, an annular stainless steel tube was installed, which permitted vertical motion of the stirrer and functioned as a water cooling jacket, as well as maintaining the vacuum at all times. Within the stainless steel tube, a stainless steel rotating shaft, which was attached to a ferrofluidic seal shaft, was immersed. This shaft was connected to the stirring paddle.

In order to maintain a constant seal, the water cooled jacket was welded to a flange, which in turn was fastened to the ferrofluidic casing. The rotational movement of the inner shaft was provided by a variable speed motor connected by a belt to the pulley and was mounted in the rotating shaft. The total assembly was coupled to a hydraulic piston which provided vertical motion of the paddle.

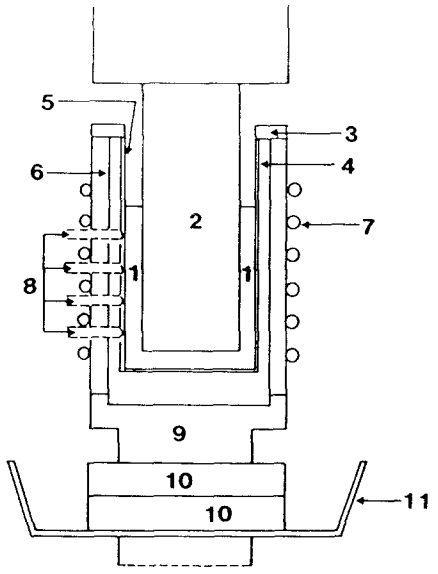

Figure 2 Details of the crucible assembly of the rheocasting vacuum furnace. 1, Partially solidified IN–100 2, alumina paddle; 3, pyrolitic graphite plate; 4, graphite susceptor; 5, alumina crucible; 6, fibrefrax; 7, water cooled induction coils; 8, thermocouples; 9, pyrolitic graphite plate; 10, alumina plates; 11, stainles steel pan.

The crucible and the stirring paddle were made of high density and high purity alumina (Al_2O_3). The crucible had an inner diameter of 9.9 cm, height of 19.4 cm and wall thickness of 0.3 cm. The stirring paddle was cut to size to fit the alumina crucible, ensuring a maximum clearance of 1.3 cm on both sides and the bottom of the paddle. With such a clearance, adequate stirring was provided. The paddle has a rectangular shape and was 7.3 cm wide, 1.3 cm thick and 26.7 cm long. Both the crucible and the paddle were used only once for a given run.

Two to four W–5% Re/W–26% Re thermocouples were inserted through the wall of the graphite susceptor which touched the outside wall of the alumina crucible at different locations along its length, Fig. 2. A strip-chart recorder was used to obtain continuous temperature–time curves during melting and subsequent rheocasting. To establish the temperature difference between the liquid metal and the outside wall

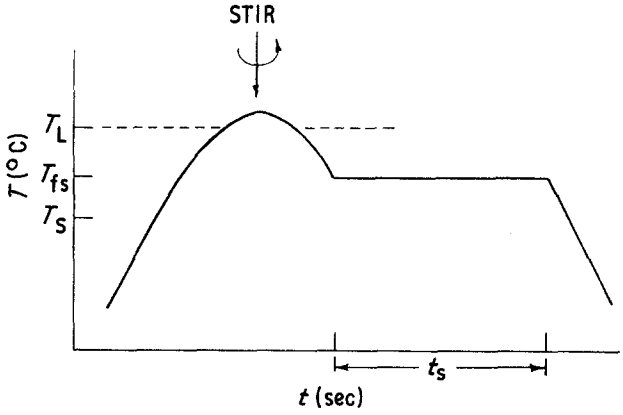

Figure 3 Graphical presentation of the process approach and the experimental variables addressed in this study.

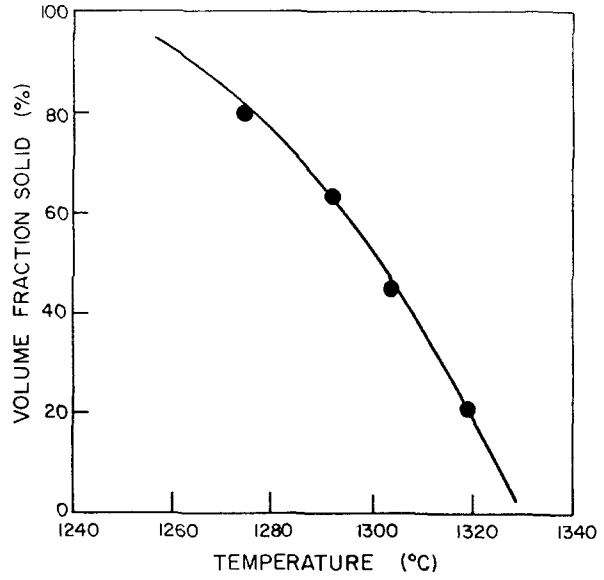

Figure 4 Estimated volume fraction solid against temperature for IN–100.

of the crucible, a temperature calibration run was made *a priori*.

The processing approach followed and the variables which were evaluated are shown in Fig. 3. In order to obtain the relationship of volume fraction solid as a function of temperature, a differential thermal analysis (DTA) of the starting material was carried out at Special Metals Corporation. Three samples in the as-received VIM condition were analysed. The resultant volume fraction solid (f_s) present in the slurry as a function of temperature in the mushy zone, is shown in Fig. 4.

The process variable levels examined are:

1. fraction solid, f_s, maintained at 35 and 65%;
2. stirring speed, γ_s, stirred at 325 and 560 r.p.m.;
3. isothermal stirring time, t_s, held for 15 and 45 min while stirring.

The following procedure was followed during a rheocasting run. The furnace chamber was evacuated to about $4 \times 10^{-2}\,\mu$m (4×10^{-5} torr). The power to the induction unit was then turned on. In order to fully melt the charge, the power was raised to a maximum of 5 kw. Upon complete melting of the charge, the vacuum was increased to $0.6\,\mu$m (6×10^{-4} torr); this level of vacuum was maintained throughout the rheocasting operation. The paddle, which was preheated by lowering it to a position just above the melt surface, was then lowered into the melt to its proper stirring position and rotated. Simultaneously, the alloy was slowly cooled with a constant cooling rate through its solid–liquid temperature range. Upon reaching the temperature corresponding to the volume fraction solid desired, the temperature was equilibrated and the slurry was stirred for a given period of time, t_s. Finally, for runs stirred at the volume fraction solid of 35%, the paddle was immediately raised out of the crucible after the stirring was terminated and the slurry was allowed to completely solidify in the furnace. However, for runs stirred at a high volume fraction solid of 65%, the slurry became viscous and the paddle could not be raised from the slurry. As a consequence, for runs stirred at 65% f_s, the slurry was simply furnace cooled without lifting the paddle.

TABLE II Summary of rheocast runs and the corresponding processing variables maintained

Run	Volume fraction solid (f_s, %)	Stirring speed (γ_s, r.p.m.)	Isothermal stirring time (t_s, min)	
A	(unstirred and continuously cooled)			
B	35	325	15	N
C	35	560	15	N
D	35	325	45	N
E	65	325	15	P

N, ingot without paddle left in it.
P, ingot with paddle left in it.

Table II lists rheocasting runs made under different processing variables. Altogether a total of 30 rheocasting runs were made, however, representative runs for a given set of experimental variables were selected to facilitate discussion. The solidified ingots with or without the rotating paddle were sectioned for structural characterization studies and post solidification thermal treatments.

3.2.2. VADER

The microstructure and mechanical properties of the rheocast ingots were evaluated and compared to the VADER cast ingots. A schematic of the VADER melting process has been shown in Fig. 1. In the VADER process, two consumable electrodes are arced against each other with no additional power input into the remelted pool. The molten metal is allowed to drip into a mould located under the electrodes. The arc polarity can be reversed to offset the different consumption rates between the cathode and anode (about 10%). The moulds were rotated up to 100 r.p.m. to distribute the droplets and create a uniform metal meniscus. A 45.5 kg ingot of IN–100 nickel-base superalloy was produced by the VADER process at Special Metals Corporation for this study.

3.3. Structural evaluation

3.3.1. Reheating experiment

To distinguish clearly and delineate between the primary solid phase which had been present during rheocasting and the liquid phase surrounding the primary solid phase, a set of reheating experiments was carried out. The reheating experiments were carried out in a high temperature tube furnace in an argon environment. A Pt–Pt 10% Rh thermocouple was placed into the tube such that the thermocouple tip was adjacent to the sample. The sample was heated to the temperature at which it was originally rheocast, T_{fs} (see Fig. 3) and was isothermally held for a period of 5 min. Subsequently, the sample was quickly removed and water quenched. Samples from non-stirred and VADER ingots were also included in this study to compare with the rheocast samples.

3.3.2. Structural characterization

The surfaces of the ingots were ground and then macroetched in a solution of HCl, H_2O and H_2O_2 in a ratio of 5:5:2, respectively. Several samples were

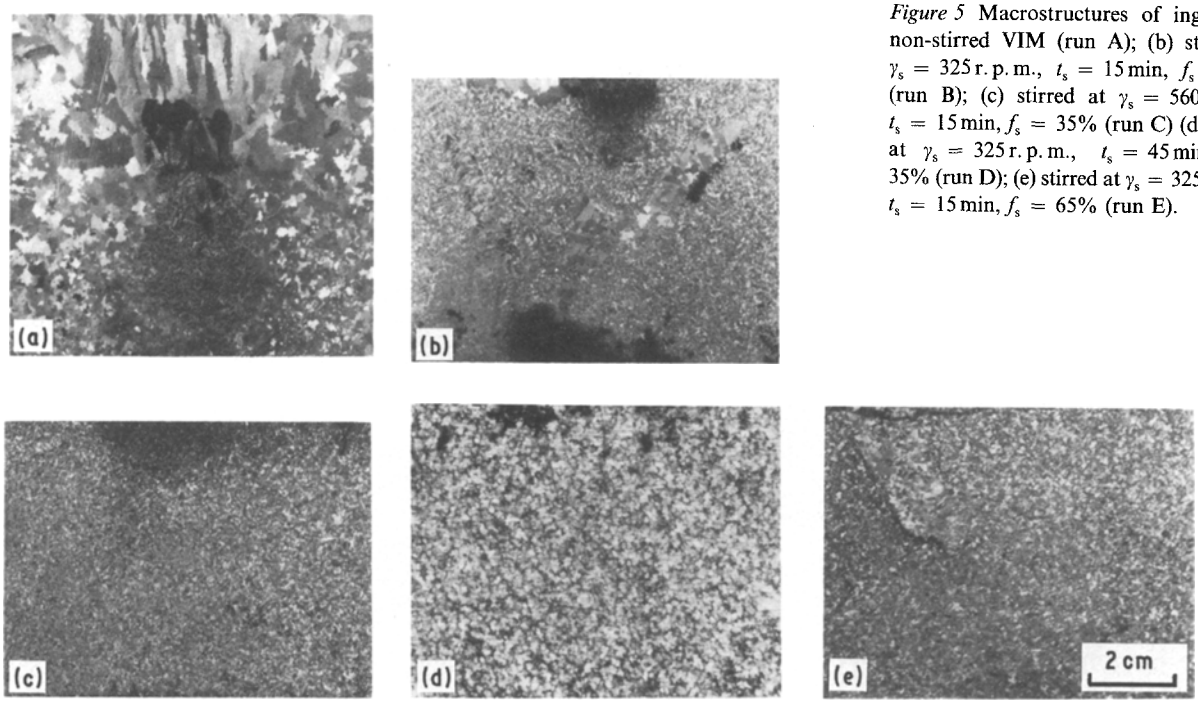

Figure 5 Macrostructures of ingots: (a) non-stirred VIM (run A); (b) stirred at γ_s = 325 r.p.m., t_s = 15 min, f_s = 35% (run B); (c) stirred at γ_s = 560 r.p.m., t_s = 15 min, f_s = 35% (run C) (d) stirred at γ_s = 325 r.p.m., t_s = 45 min, f_s = 35% (run D); (e) stirred at γ_s = 325 r.p.m., t_s = 15 min, f_s = 65% (run E).

sectioned from different locations of each ingot to study the microstructure. Glyceria etch (10 ml glycerin, 15 ml HCl and 5 ml H_2O) was used as an etchant. Optical and scanning electron micrographs were obtained at different magnifications. The K ratio profiles of segregation were studied through X-ray analysis using wavelength dispersive spectroscopy (WDS). The K ratio is an intensity ratio and is defined as follows:

$$K = \frac{\text{intensity of sample primary emission}}{\text{intensity of pure element standard primary emission}}$$

This calculated K ratio is roughly proportional to the actual composition of the solute in the alloy and is used here for relative comparison. Two solutes, titanium and chromium, were selected to characterize segregation in the cast products.

4. Results and observations

Both the macrostructure and microstructure of IN–100 alloy, processed as (i) non-stirred VIM cast, (ii) rheocast and (iii) VADER cast, are discussed below.

4.1. Macrostructure

4.1.1. Non-stirred VIM cast

The longitudinal macrostructure of a non-stirred ingot is shown in Fig. 5a; the VIM as-received charge was remelted in the rheocasting apparatus without stirring. The macrostructure of the top region of the ingot consists of columnar grains, the bottom region of fine-equiaxed grains, and the centre region of coarse-equiaxed grains accompanied with large shrinkage cavities. Many interconnected cracks exist throughout the ingot.

4.1.2. Rheocasting

The macrostructures of the various rheocast ingots of IN–100 are shown in Figs 5b–e, respectively. The effect of stirring speed on the rheocast macrostructure is seen in Figs. 5b and c, stirred at 325 and 560 r. p. m., respectively. In both cases, the stirring time and the volume fraction solid were kept fixed at 15 min and 35% volume fraction solid. For an ingot of low stirring speed, i.e. 325 r.p.m., the macrostructure shows a non-uniform distribution of grain size and morphology (Fig. 5b). The coarse grains are accumulated as a "V" shape near the centre, while the fine grains are distributed close to the edge and at the bottom of the ingot. Many intergranular pores are observed in the sample stirred at 325 r.p.m. As the stirring speed increases from 325 to 560 r. p. m., grain size and morphology becomes more uniform, cf. Figs 5b and c. It is clear that large grains are not observed in the sample stirred at high speeds. Moreover, there is a marked decrease in the amount of intergranular pores in the sample stirred at 560 r.p.m. compared with the one stirred at 325 r.p.m., see Figs 5b and c. In all the macrostructures shown in Figs 5b and c, large shrinkage cavities were not observed.

The effect of isothermal stirring time on the resultant rheocast macrostructure, while the volume fraction solid (35%) and stirring speed (325 r. p. m.) were kept constant, can be seen by comparing the structures shown in Figs 5b and d. It can be seen that as the stirring time is increased from 15 min (Fig. 5b) to 45 min (Fig. 5d), coarse grains and shrinkage cavities disappear, and a more homogeneous grain size distribution is obtained.

The effect of the isothermal temperature at which the melt/slurry was held for a given time during rheocasting on the resultant structure is significant. Samples were held in the mushy zone at 1312° C (35% f_s) and 1295° C (65% f_s) while the stirring time and the stirring speed were kept constant at 15 min and 325 r.p.m. Figs 5b and e show the macrostructures of rheocast ingots at 35 and 65% f_s, respectively. Both Figs 5b and e show regions of large grains surrounded by fine ones. However, the amount of large grains decreases as the volume fraction solid increases; in

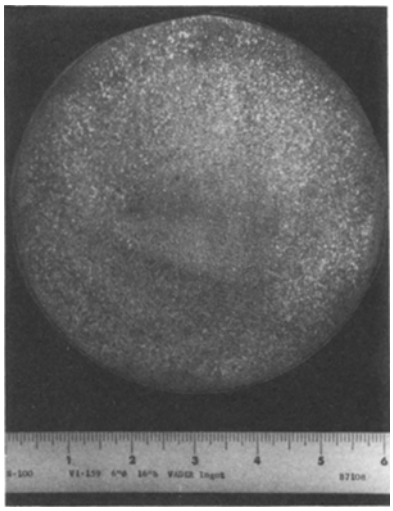

Figure 6 Macrostructure of VADER processed IN–100.

essence a more uniform grain size distribution is obtained if the slurry is rheocast at a high volume fraction solid.

4.1.3. VADER

Fig. 6 is a representative macrostructure of a 15.3 cm diameter VADER IN–100 ingot. The macrostructure is characterized by a uniform distribution of fine and equiaxed grains. Neither cavities nor intergranular cracks were found in the VADER processed ingot.

4.2. Microstructure

4.2.1. Non-stirred VIM cast

Fig. 7a is the microstructure representative of the fine-grained region of the non-stirred ingot. The grains are clearly dendritic with a dendrite arm spacing of $\sim 120\,\mu m$. The voids are located randomly along interdendritic regions and grain boundaries.

TABLE III Concentration and segregation ratio

Run	Titanium (K, %)			Chromium (K, %)		
	C_0	C_{mid}	S	C_0	C_{mid}	S
A						
Mean	3.03	3.96	1.31	10.91	11.63	1.07
S.D.*	0.30	0.11	0.09	0.28	0.11	0.02
S.E.†	0.06	0.02	0.02	0.06	0.02	0.01
B						
Mean	3.29	3.97	1.20	11.06	11.68	1.06
S.D.	0.15	0.19	0.11	0.22	0.11	0.01
S.E.	0.03	0.04	0.03	0.04	0.02	0.01
C						
Mean	3.29	3.97	1.20	11.07	11.67	1.05
S.D.	0.13	0.09	0.03	0.20	0.09	0.01
S.E.	0.03	0.02	0.01	0.04	0.01	0.01
D						
Mean	3.41	4.01	1.18	11.13	11.68	1.05
S.D.	0.23	0.14	0.04	0.17	0.10	0.01
S.E.	0.05	0.03	0.01	0.04	0.02	0.01
E						
Mean	3.54	4.05	1.15	11.29	11.63	1.03
S.D.	0.09	0.05	0.03	0.02	0.05	0.01
S.E.	0.02	0.01	0.01	0.01	0.01	0.01

*Standard deviation; †standard error of the mean.

The phases found in the IN–100 ingot consist of primary or eutectic γ–γ' islands and scriptlike MC carbides which are all surrounded by secondary precipitates γ' in a matrix of γ. The γ–γ' eutectic islands, located at the interdendritic areas and grain boundaries, vary in size and shape and are non-uniformly distributed in the unstirred ingot.

The segregation ratio, S, is in general defined as C_{max}/C_0 where C_{max} is the highest solute content and C_0 is the lowest solute content in a dendrite or grain. However, due to the complexity of the grain boundary phase, the actual segregation ratio in a dendrite or

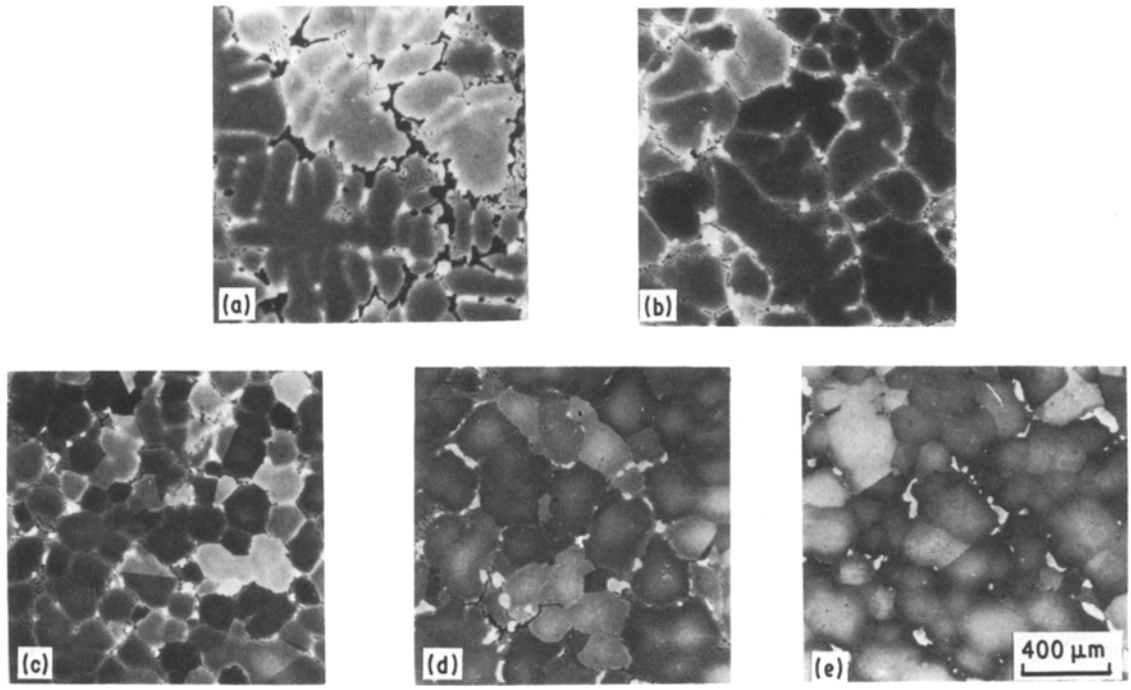

Figure 7 Representative microstructures of ingots: (a) non-stirred VIM (run A); (b) stirred at $\gamma_s = 325$ r.p.m., $t_s = 15$ min, $f_s = 35\%$ (run B); (c) stirred at $\gamma_s = 560$ r.p.m., $t_s = 15$ min, $f_s = 35\%$ (run C); (d) stirred at $\gamma_s = 325$ r.p.m., $t_s = 45$ min, $f_s = 35\%$ (run D); (e) stirred at $\gamma_s = 325$ r.p.m., $t_s = 15$ min, $f_s = 65\%$ (run E).

grain is difficult to obtain. Therefore, the composition ratio, $S = C_{mid}/C_0$ where C_{mid} is the solute content at the midpoint between the centre and boundary of a dendrite or grain, was selected to compare segregation levels. Table III illustrates the segregation ratio of chromium and titanium in the non-stirring ingot. Among 20 arbitrarily chosen dendrite arms, the measured segregation ratios show scatter for both chromium and titanium. This variation in segregation ratio can be attributed to the variation in the sectioning plane of the dendrites.

4.2.2. Rheocasting

Figs 7b–e show the microstructures of various rheocast IN–100 ingots. These rheocast structures clearly show that the structure is nondendritic. The effect of stirring speed on the rheocast microstructure is seen in Figs 7b and c. At a low stirring speed of 325 r. p. m., most of the dendritic structure that was observed in the non-stirred ingot has been replaced by rosette-like and spherical particles (Fig. 7b). As the stirring speed increases from 325 to 560 r. p. m., one can note that the transition from dendritic to spherical particles is more prevalent, see Figs 7b and c. In Fig. 7c, the sample stirred at 560 r. p. m. exhibits predominantly spherical particles in the order of 120 μm. Moreover, as the stirring speed increases, the observed grain size and interparticle voids decrease; in addition, one notes a more homogeneous distribution of grains. The amount of γ–γ' eutectic islands and carbide particles along the grain boundaries is not affected by the stirring speed; however, the homogeneity of the γ–γ' island distribution and their size is affected: at 560 r. p. m. one observes a more homogeneous distribution of γ–γ' eutectic islands and smaller size islands than at a stirring speed of 325 r. p. m.

Effect of stirring speed on the segregation ratio is illustrated by comparing the segregation ratio in the ingot which was obtained at a stirring speed of 560 r. p. m. to that in the ingot which was obtained at a stirring speed of 325 r. p. m. (Table III). At a constant stirring time and volume fraction solid, there is no significant difference in the segregation ratio as the stirring speed increases.

The effect of the isothermal stirring time on the resultant rheocast microstructure is seen by comparing the micrographs shown in Figs 7b and d. The majority of the grains shown in Fig. 7d are spherical. The average grain size is approximately 160 μm (Fig. 7d), which is larger than the dendrite arm spacing of 120 μm for the non-stirred casting shown earlier in Fig. 7a. A comparison of Figs 7b and d reveals that both the grain size and the amount of the interparticle voids decrease as the isothermal stirring time increases. In addition, varying the isothermal stirring time does not affect the amount and size of the γ–γ' eutectic islands and carbide particles; however, the distribution of γ–γ' eutectic islands is more uniform in those samples, which were isothermally stirred for a longer time, i.e. 45 min.

Table III also shows the segregation ratio in the rheocast ingot which was obtained by stirring the slurry at a speed of 325 r. p. m., volume fraction solid

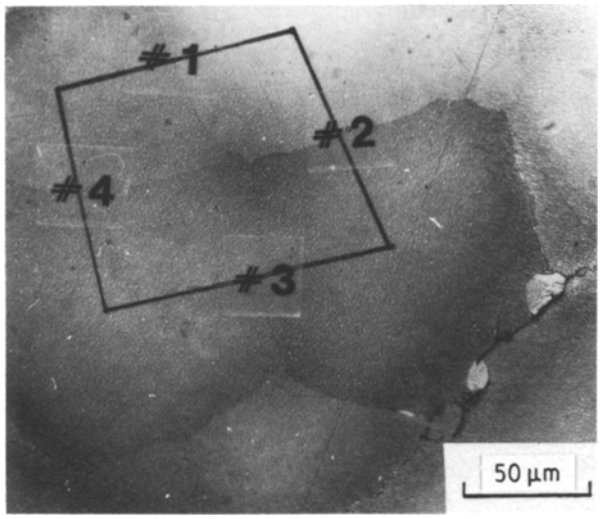

Figure 8 Representative optical micrograph of an agglomerate in ingot (run E) at a high magnification.

of 35% and a stirring time of 45 min. Comparing the segregation ratio of rheocast ingots stirred at 45 and 15 min, it can be seen (Table III) that increasing the stirring time does not significantly change the segregation ratio, S, of titanium and chromium.

Figs 7b and e show the microstructures of rheocast ingot at volume fractions solid of 35% and 65%, respectively, where the stirring speed and isothermal stirring time were kept constant. It can be seen that as the volume fraction solid increases, the rosette-like morphology of the primary phase decreases. Furthermore, change in volume fraction solid from 35% f_s to 65% f_s results in a decrease in grain size.

Some grains in the ingots, which were stirred at 65% f_s are observed to be joined together to form agglomerates, Fig. 7d. Fig. 8 shows the representative optical micrograph of an agglomerate observed at high magnification. This agglomerate exhibits four grain boundaries, which are designated 1 to 4. The titanium K ratio profile across all four boundaries is shown in Fig. 9. It is noted that grain boundaries 1 to 4 are all titanium enriched.

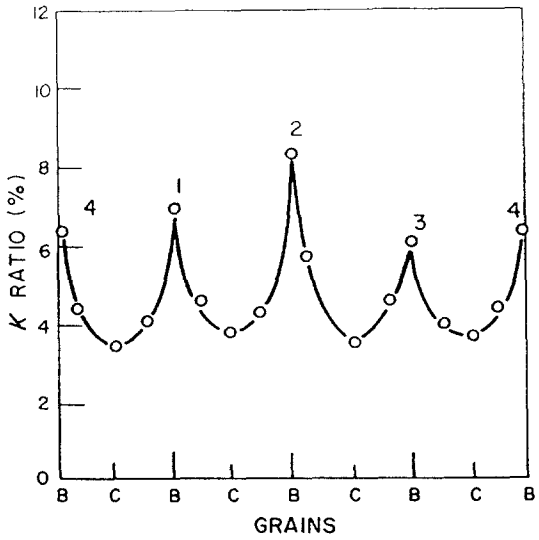

Figure 9 Titanium concentration profile across grain boundaries 1, 2, 3 and 4 indicated in Fig. 8. B denotes measurement taken near grain boundary; and C denotes measurement taken at grain centre.

TABLE IV Effect of stirring variables on the rheocast structure

Processing variables	Primary solid particle		Segregation		Grain		$\gamma-\gamma'$ eutectic phase		
	Size	Sphericity	Macro	Micro	Size	Sphericity	Size	Amount	Uniformity of distribution
Rising r_s	−	+	−	0	−	+	−	0	+
Rising t_s	−	+	−	−	−	+	0	−	+
Rising f_s	−	+	−	−	−	+	0	−	0

+, increase; −, decrease; 0, no change.

The size and amount of the $\gamma-\gamma'$ eutectic islands are influenced by the volume fraction solid present during the isothermal hold time in the mushy zone. A comparison of Figs 7b and e shows that the size and amount of the $\gamma-\gamma'$ eutectic island decreases as the volume fraction solid increases. However, no variation is observed in the morphology of the carbide particles as the volume fraction solid changes, c.f. Figs 7b and e.

Comparing the segregation ratio in a rheocast ingot while isothermally stirred at a volume fraction solid of 65% (Table III) to another rheocast ingot while isothermally stirred at a volume fraction solid of 35% (Table III), it can be noted that for a constant stirring speed and time, the segregation ratio decreases as the volume fraction solid increases. In addition, both solute content of C_0 and C_{mid} increases by increasing the volume fraction solid.

In summary, the effect of stirring speed, isothermal stirring time and volume fraction solid on the resultant macro- and microstructural features are listed in Table IV.

4.2.3. VADER

The microstructure of VADER samples lacks identifiable spines, and can be categorized as consisting of a group of equiaxed nondendritic grains (Fig. 10). A grain size of approximately 100 μm in the VADER ingot is less than the grains measured in the rheocast ingots (Figs 7b to e). The size and distribution of the phases which are present in the VADER IN–100 are shown in Fig. 10. The $\gamma-\gamma'$ eutectic islands are uniformly distributed and vary in size and shape. The size of the $\gamma-\gamma'$ islands observed in the VADER ingot (Fig. 10) is similar to that observed in the rheocast ingot stirred at a speed of 560 r.p.m. (Fig. 7c); however, the size of the $\gamma-\gamma'$ islands is smaller than those observed in all the rheocast ingots (Figs 7b, d and e).

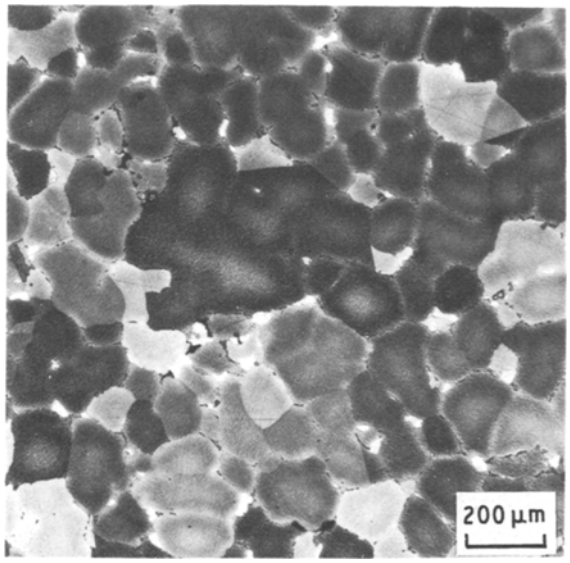

Figure 10 Representative microstructure of VADER processed IN–100.

The representative segregation ratios in the VADER ingot are shown in Table III. The segregation ratios in the VADER ingot are similar to those found in the non-stirred ingot.

5. Discussion

5.1. Observation of primary solid particles

The primary solid particles, present in the alloy when it was partially solid, have coarsened and changed morphology during subsequent solidification in the crucible. Therefore, in order to delineate the size and morphology of these primary solid particles, samples sectioned from non-stirred, VADER and rheocast ingots were reheated and quenched. The imposed high solidification rate enables us to delineate and distinguish between the primary solid phase and the surrounding liquid phase. The primary solid particles in this duplex structure may be different from those existing during rheocasting due to the substantial coarsening and homogenization that takes place during furnace cooling subsequent to rheocasting.

Duplex structures of reheated specimens from non-stirred, rheocast and VADER ingots are shown in Fig. 11. Fig. 11a illustrates the duplex structure of the reheated sample which was non-stirred. In the absence of stirring, the observed primary solid particles are typical to those found in conventional dendritic structures.

The effect of stirring speed at constant stirring time (15 min) and constant volume fraction solid (35%) on the primary solid particles is seen in Figs 11b (325 r.p.m.) and 11c (560 r.p.m.). In Fig. 11b, the primary solid particles exhibit combinations of dendritic, rosette-like and spherical morphologies; while in Fig. 11c only spherically shaped primary solid particles are seen. It is quite clear that the higher the stirring speed, the primary solid particles are finer and more spherical.

Figs 11b and d show the effect of isothermal stirring time of 15 and 45 min, respectively, on the morphology of the primary solid particles at constant stirring rate (325 r.p.m.) and volume fraction solid (35%). It can be noted that sphericity and number of primary solid particles increases as the stirring time increases. However, when comparing the reheated structure resulting from a prolonged stirring action, Fig. 11d, with that of high stirring speed at a constant volume fraction solid, Fig. 11c, it is clear that the former exhibits coarser

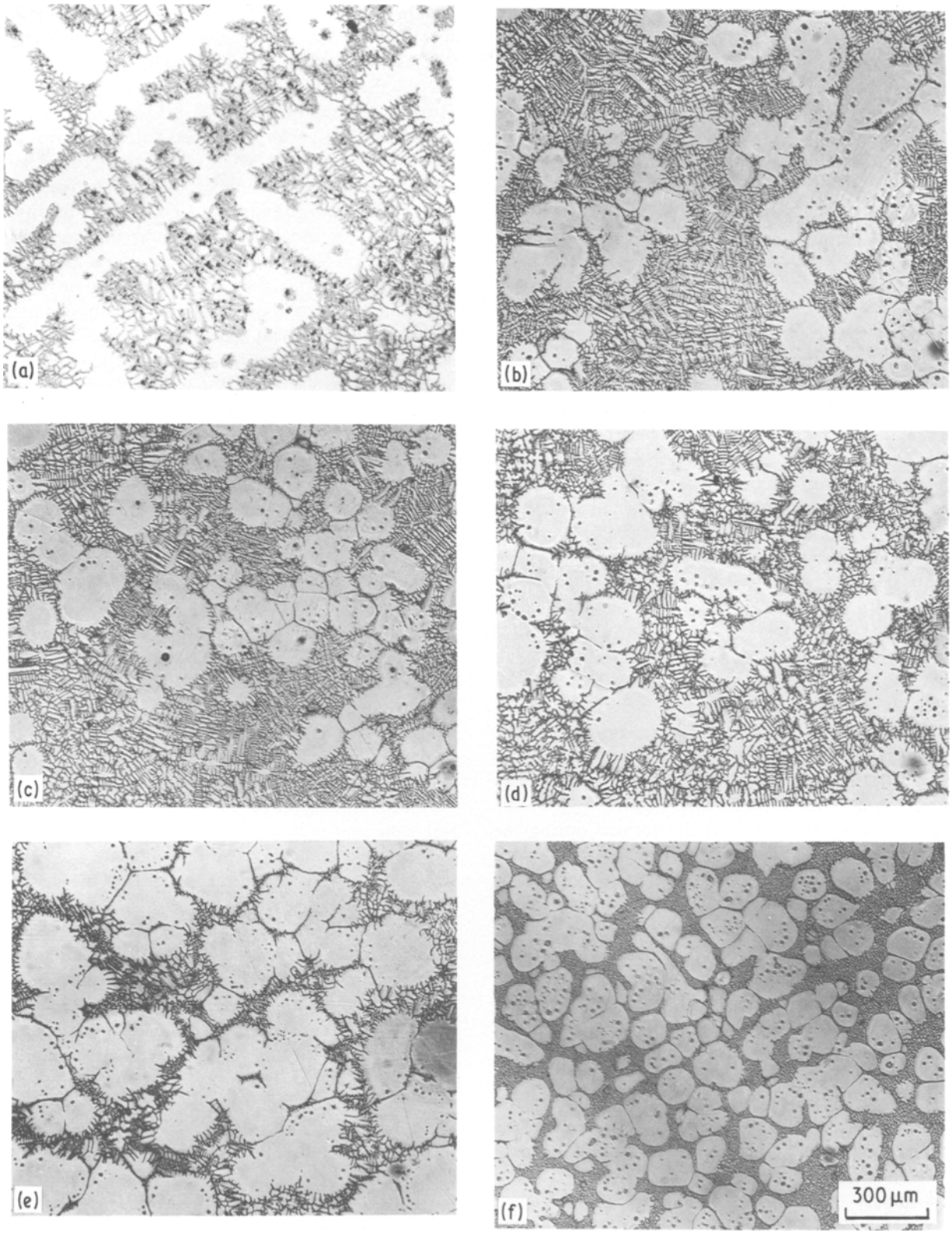

Figure 11 Representative microstructures of reheated samples: (a) non-stirred VIM (run A); (b) stirred at γ_s = 325 r.p.m., t_s = 15 min, f_s = 35% (run B); (c) stirred at γ_s = 560 r.p.m., t_s = 15 min, f_s = 35% (run C); (d) stirred at γ_s = 325 r.p.m., t_s = 45 min, f_s = 35% (run D); (e) stirred at γ_s = 325 r.p.m., t_s = 15 min, f_s = 65% (run E); (f) VADER.

primary solid particles than the latter. This indicates that coarsening will be accelerated more by a prolonged stirring action rather than by a high stirring speed.

The effect of volume fraction solid at constant stirring speed and constant isothermal stirring time on the morphology of the primary solid particles is illustrated in Figs 11b (35% f_s) and 11e (65% f_s). The primary solid particles at high volume fraction solid tend to sinter together and form agglomerates. Many partially wetted particle boundaries are observed in each agglomerate in Fig. 11e while the particle boundaries shown in Figs 11b and c are completely wetted. It can be noted that coarsening and dendrite fragmentation increases as the volume fraction solid increases.

A specimen sectioned from the VADER ingot was reheated to a temperature corresponding to a volume fraction solid of 65%, isothermally held for 5 min and

was subsequently water quenched. The primary solid particles are fine, spherical and uniformly distributed in the reheated structure, Fig. 11f. Dendritic particles were not observed in the reheated VADER sample. The size of the primary solid particles observed in the VADER sample (Fig. 11f) is smaller than the size of the primary solid particles observed in the rheocast ingot, which was stirred at 325 r. p. m., 15 min and 65%f_s (Fig. 11e).

5.2. Structural evolution

5.2.1. Rheocasting

From the observation and results of various reheated structures, it is clear that the conventional dendritic morphology of the primary solid particles is transformed to one consisting of rosette-like or spherical shaped particles by the introduction of mechanical stirring during solidification. The change from a dendritic to the rounded globular morphology is due to dendrite bending, fragmentation and subsequently coarsening during the vigorous stirring and isothermal holding of the slurry. A detailed description of dendrite fragmentation and grain boundary movement during rheocasting in IN–100 is given by Cheng *et al.* [6].

5.2.1.1. Effect of stirring speed. When the IN–100 melt is continuously stirred by a rectangular paddle from 30° C above T_L to a temperature slightly below T_L (Fig. 3), the nuclei which form are uniformly suspended in the melt; the gravity effect resulting from density differences between the solid and liquid phases is overcome by the induced fluid flow.

The primary dendrite particles formed during the early stages of solidification exhibit a low solute content and are plastically deformable under shear near the alloy's melting point [26]. Dendrite arms of the primary solid particles are bent by the stirring induced shear stresses and form grain boundaries [25]. Consequently, nondendritic particles will be formed since the dendrites will break apart along the prior boundaries [25]. These solid particles then spheroidize during isothermal holding in the mushy zone.

The effect of stirring speed on the resultant rheocast structure is shown in Figs 5b, 7b, 5c and 7c. Increasing the stirring speed in the liquid metal increases the turbulent fluid flow and therefore results in an increase in the induced shear stress on the dendrite particles. Accordingly, the amount of solid particles detached from the dendrites by fragmentation increases as the speed of mechanical stirring increases. Therefore, at a high stirring speed of 560 r. p. m., most of the primary solid particles present after an isothermal hold are spherical in shape, Fig. 11c, while in a low stirring speed of 325 r. p. m., the primary solid particles show a combination of dendritic, rosette-like and spherical morphologies, Fig. 11b.

The macrosegregation of the resultant rheocast structure has been eliminated by increasing the stirring speed during processing, c.f. Figs 5b and c. This effect of stirring speed on the macroscale chemical homogeneity can be attributed to the degree of mass feeding, i.e. movement of solid and liquid, when the paddle was removed from the melt. For all ingots stirred at a volume fraction solid of 35%, the stirring was discontinued after isothermal holding, and subsequently the rectangular paddle was lifted out and the slurry was allowed to cool. The primary solid particles suspended fully in the liquid metal during stirring will tend to cluster together when the stirring is terminated. The strength (or number) of bonds between particles increases with time and so does the viscosity of the slurry. Moreover, it has been shown that the clustering reaction is faster in a slurry with a large amount of solid–liquid interfacial area, e.g. dendritic or rosette-like solid particles, than in a slurry having a smaller solid–liquid interfacial area, e.g. spherical solid particles [25]. Accordingly, for a liquid metal stirred at a high speed of 560 r. p. m., the resultant primary solid particles are mostly spherical as seen in Fig. 11c; these particles can easily rearrange their positioning, i.e. mass feeding occurs. In contrast, as the stirring speed decreases from 560 to 325 r. p. m., the number of rosette-like solid particles increases, giving rise to an increase in viscosity. Since mass feeding of the slurry stirred at 325 r. p. m. is now more difficult, when lifting the stirring paddle, a V shaped region with only a few primary solid particles forms in the core of the ingot. After the slurry is furnace cooled, coarse equiaxed dendritic grains form in this V shaped region since only a few nuclei are present (Fig. 5b).

Increasing the stirring speed in the mushy zone does not significantly change the level of microsegregation (Table III) because the total solidification time including the isothermal hold in the mushy zone does not vary with stirring speed. At constant isothermal stirring time and volume fraction solid, the amount of γ–γ' eutectic islands present in the resultant rheocast structure does not change as the stirring speed varies. However, changing the stirring speed affects the size and morphology of grains in the ingot and therefore gives rise to a change in the size and distribution of the γ–γ' eutectic islands. For the ingot rheocast at a low speed of 325 r. p. m., a significant amount of the existing rosette-like or dendritic grains exhibit fine γ–γ' eutectic particles between the bent dendrites and coarse particles between grains, Fig. 7b. In contrast, as the stirring speed increases the amount of spherical grains increases, thus the number of grain boundaries increases. Consequently, the γ –γ' eutectic islands will precipitate uniformly between the grains. Similarly, the distribution of the microporosity is expected to be more uniform in the ingot which was stirred at higher speeds than the ingot processed at lower stirring speeds.

5.2.1.2. Effect of isothermal stirring time. Increasing the isothermal stirring time improves the macro- and microsegregation, grain refinement and morphology of the rheocast ingot, c.f. Figs 5b, 7b, 5c and 7c. This improvement on the resultant rheocast structure can be attributed to the enhanced dendrite fragmentation and coarsening which takes place in the primary solid particles, as the isothermal stirring time in the mushy zone increases.

Most of the bent dendritic or rosette-like primary

solid particles found at a short isothermal stirring time of 15 min (Fig. 11b) have been replaced by the spherical primary solid particles as the stirring time increases to 45 min, (Fig. 11d). Clearly the longer the slurry is stirred, the more the dendrite arms are plastically deformed by the induced shear stresses. The number of primary solid particles has been seen to increase as the isothermal stirring time increases; however, the primary particle size in the ingots stirred for longer times (Fig. 11d), is larger than bent dendrite arms or particles in the ingots stirred for shorter times, (Fig. 11b). This increase in the size of primary particles can be attributed to the enhanced coarsening resulting from longer isothermal holding times.

Macrosegregation in the rheocast ingot is reduced by increasing the isothermal stirring time during solidification. This is because increasing the stirring time increases the amount of spherical primary solid particles at the same volume fraction solid and facilitates mass feeding as the paddle is pulled out from the slurry.

Increasing the isothermal stirring time clearly increases the time available for solute diffusion to occur in the primary solid particles. Therefore, the solute content can be expected to be more homogeneous and close to the equilibrium composition in the primary solid particles after 45 min of isothermal stirring than in those particles which have been isothermally stirred for 15 min (Table III). In addition, the distribution of the $\gamma-\gamma'$ eutectic islands in the rheocast ingot becomes uniform as the isothermal stirring time increases, Figs 7b to d.

5.2.1.3. Effect of volume fraction solid. At a constant isothermal hold time and stirring speed, the degree of segregation in the resultant rheocast ingot decreases as the volume fraction solid increases. In addition, increasing the volume fraction solid reduces the grain size and improves the sphericity of the grains. These improvements in the rheocast structure by changing the volume fraction solid can be attributed to (i) increasing stirring time; (ii) increasing the induced shear stresses on the dendrite arms; and (iii) increasing the solute concentration gradient.

In order to keep a constant cooling rate of $4^\circ C\,min^{-1}$, the time spent on cooling from the liquidus temperature, T_L, to the desired temperature, T_{fs}, increases as the T_{fs} decreases. Therefore, the total stirring time is longer in the ingot isothermally stirred at 65% f_s than at 35% f_s. Furthermore, the apparent viscosity of the slurry clearly increases as the volume fraction solid increases [4]. Accordingly, in order to keep a constant stirring speed of the paddle, the amount of the power or shearing needed to agitate the slurry of a higher viscosity (a higher volume fraction solid) is higher than that needed to agitate the slurry of a lower viscosity (a lower volume fraction solid). Therefore, the dendrite arms can be expected to be subjected to an increasing shear stress as the volume fraction solid increases. Thus, dendrite arm fragmentation occurs more readily and the spherical morphology of primary solid particles is more stable in slurries stirred at 65% f_s, (Fig. 11e) than those stirred at 35% f_s, (Fig. 11b).

All spherical primary solid particles observed in the specimen of a high volume fraction solid of 65% (Fig. 11e) are not isolated, and instead they tend to coalesce and form agglomerates. Moreover, in the rheocast structure the number of the agglomerates observed increases as the volume fraction solid increases, cf. Figs 7b and e. This agglomeration of the spherical or rounded particles is believed to result from particle collision during stirring. Increasing the volume fraction solid in the mushy zone shortens the interparticle distance and thus can enhance the possibility of interparticle collisions. The representative composition profile obtained inside an agglomerate of the rheocast structure (Fig. 8) confirms that all boundaries observed inside this agglomerate are segregated boundaries.

For ingots stirred at a high volume fraction solid of 65%, the stirring paddle was left in the slurry during furnace cooling because it could not be lifted out. Thus, the V shaped region of coarse equiaxed dendritic grains is absent in these ingots. Instead, the primary solid particles which were uniformly distributed during stirring tend to sink due to gravity effects. This gives rise to regions of coarse equiaxed-dendritic grains at the top of the ingots (Fig. 5e).

Microsegregation of the rheocast ingot is reduced by increasing the volume fraction solid (Table III). During solidification, as the volume fraction solid increases, the difference of solute content between the centre and boundary of a solid particle increases (neglecting solute diffusion in the solid), and therefore results in an increasing solute concentration gradient in the solid particles. It is assumed here that the particle size does not significantly change with varying volume fraction solid. On subsequent isothermal stirring, the solute content at the particle centre will increase because an increasing solute concentration gradient in a particle will give rise to an increasing net flux of solute atoms transported from particle boundary to centre. Consequently, the resultant rheocast grains in ingots stirred at a higher volume fraction solid (Table III) show a more homogeneous solute distribution, i.e. a higher solute content in the grain centre and a lower segregation ratio, than those in ingots stirred at a lower volume fraction solid.

5.2.2. VADER

The resultant macro- and microstructures of the VADER processed ingot, Figs 6 and 10, are significantly different from those observed by conventional ingot processing. Since in the VADER process the semi-liquid mass is continually being fed by the falling droplets, there are no gravity effects resulting from density differences between the solid and the liquid phases. The numerous solid particles or nuclei will then be uniformly distributed throughout the slurry, which is similar to the rheocasting process where no distinct liquid pool or liquidus isotherms exist. As a consequence, a uniform nondendritic grain size and a reduced level of macrosegregation is obtained in the VADER ingot.

The grain size obtained by the VADER process (Fig. 10) is smaller than the grain size observed in the

rheocast ingots (Figs 7b–e). This difference in the grain size between the two processes can be attributed to the following causes.

(i) the cooling rate in the VADER process (metal droplets were dripped into a slowly rotated steel mould) is faster than that in rheocasting (metal slurry is solidified in the alumina crucible);

(ii) there exist more nuclei in the VADER slurry than in the rheocast slurry. This is confirmed by comparing the structure shown in Figs 11f and e; at the same volume fraction solid of 65%, there are more primary solid particles in the VADER ingot than in the rheocast ingot;

(iii) grain coarsening can be enhanced by mechanical stirring during rheocasting [27] which does not occur during VADER processing.

6. Conclusions

1. Mechanical stirring during solidification of IN–100 superalloy results in a cast product having a nondendritic structure. This is because under the induced shear stresses the dendrites plastically bend and recrystallize, and grain boundaries fragment.

2. The degree of structural enhancement inherent in rheocast ingots is influenced by three processing variables: stirring speed, isothermal stirring time and temperature or volume fraction solid held in the mushy zone. The general trends established, reflecting the effect of processing variables on the resultant rheocast structure, are: (i) increasing the stirring speed increases the amount of dendrite arm deformation and fragmentation resulting in an increasing number of primary solid particles, i.e. a decrease in particle size, at a constant volume fraction solid and isothermal stirring time. This decrease in particle size resulting from increasing stirring speed provides mass feeding during lifting of the stirring paddle. In turn, this gives rise to an increasingly uniform distribution of fine grains and grain boundary phases in the resultant rheocast ingot. The level of microsegregation does not significantly change by varying the stirring speed. (ii) Increasing the stirring time refines the primary solid particles. However, coarsening is enhanced by increasing stirring time which may not be desirable. (iii) Grain refinement and structural improvement are achieved by increasing the volume fraction solid at a constant stirring speed and constant isothermal stirring time. This occurs because of an increase in the shear forces on the dendrites and also an increase in the total stirring time with an increasing volume fraction solid. An increasing volume fraction solid thus greatly reduces the level of microsegregation. However, increasing the volume fraction solid increases the opportunity for inter-particle collision and therefore raises the number of agglomerates.

3. The VADER process produces superalloy ingots which have a uniform fine grain size. This is attributed to the numerous nuclei that exist in the falling droplets. The grain size in the VADER ingot is smaller than the dendrite arm spacing of the non-stirred ingot and the grain size in the rheocast ingot.

Acknowledgements

This work was carried out under NASA contract number NAG 3-14. The authors are grateful to Mr Tom Glasgow and Dr Hugh Grey of NASA Lewis Research Centre for their encouragement and support. We are also grateful to Professor Roger Doherty of Drexel University for many helpful discussions.

References

1. J. B. MOORE and R. L. ATHEY, U.S. Patent No. 3 519 503 (1970).
2. W. J. BOESCH, J. K. TIEN and T. E. HOWSON, *Metal Prog.* **122** (1982) 149.
3. W. J. BOESCH, G. E. MAURER *and* C. B. ADASCZIK, presented at Conference on High Temperature Alloys for Gas Turbine at The Palais de Congrès, Liege, Belgium, October 1982.
4. M. C. FLEMINGS, R. G. RIEK and K. P. YOUNG, *Mat. Sci. Eng.* **25** (1976) 103.
5. J. A. CHENG, PhD thesis, Drexel University, June (1985).
6. J. A. CHENG, D. APELIAN and R. D. DOHERTY, *Met. Trans.*, in press.
7. C. T. SIMS, *J. Metals* **18** (1966) 1119.
8. R. F. DECKER and C. T. SIMS, in "The Superalloys", edited by C. T. Sims and W. C. Hagel (John Wiley, New York, 1972) p. 33.
9. J. R. MIHALISIN, C. G. RIEBER and R. T. GRANT, *Trans. Met. Soc. AIME* **242** (1968) 2399.
10. G. S. COLE and R. S. CREMISIO, in "The Superalloys" edited by C. T. Sims and W. C. Hagel (John Wiley, New York, 1972) p. 479.
11. R. F. DECKER,"Steel Strengthening Mechanisms" (Climax Moly. Co., Greenwich, USA, 1969).
12. F. H. SOYKAN and J. S. HUNTINGTON, U.S. Patent No. 4 261 412 (1981).
13. D. APELIAN, in "Advanced Casting Technology", AGARD Conference Proceeding No. 325 (NATO, Nevilly Sur Seine, 1982) p. 6/1–14.
14. M. C. FLEMINGS, in Proceedings of a Workshop held at the Army Materials and Mechanics Research Center, Watertown, Massachussetts, USA, January 1978 (Metals and Ceramics Information Center, Battelle) p.3.
15. R. A. JOLY and R. MEHRABIAN, *J. Mater. Sci.* **11** (1976) 1393.
16. A. VOGEL, PhD thesis, University of Sussex (1977).
17. R. MEHRABIAN and M. C. FLEMINGS, *Trans. AFS* **80** (1972) 173.
18. H. I. LEE, PhD thesis, University of Sussex (1982).
19. E. F. FASCETTA, R. C. RIEK, R. MEHRABIAN and M. C. FLEMINGS, *Trans. AFS* **81** (1973) 95.
20. D. B. SPENCER, R. MEHRABIAN and M. C. FLEMINGS, *Met. Trans.* **3** (1972) 1925.
21. R. G. RIEK, A. VRACHNOS, K. P. YOUNG, N. MATSUMOTO and R. MEHRABIAN, *Trans. AFS* **83** (1975) 25.
22. Y. V. MURTY, D. G. BACKMAN and R. MERHRABIAN, in Proceedings of a Workshop held at the Army Materials and Mechanics Research Center, Watertown, Massachussetts, USA, January 1978 (Metals and Ceramics Information Center, Battelle) p. 95.
23. V. LAXMANAN, MSc thesis, Massachusetts Institute of Technology, (1975).
24. T. Z. KATTAMIS, U. T. HOLMBERY and M. C. FLEMINGS, *J. Inst. Metals* **95** (1967) 343.
25. R. D. DOHERTY, H-I. LEE and E. A. FEEST, *Mat. Sci. Eng.* **65** (1984) 181.
26. A. VOGEL and B. CANTOR, *J. Crystal Growth* **37** (1977) 309.
27. A. VOGEL, R. D. DOHERTY and B. CANTOR, in Proceedings of the International Conference on Solidification, University of Sheffield, England, July 1977, (The Metal Society, London) p. 518.

Received 14 January
and accepted 13 March 1986